Additive-Free Bulk-Heterojuction Solar Cells with Enhanced Power Conversion Efficiency, Comprising a Newly Designed Selenophene-Thienopyrrolodione Copolymer

*Dong Hwan Wang, Agnieszka Pron, Mario Leclerc, and Alan J. Heeger**

Bulk-heterojunction solar cells are reported with an enhanced power conversion efficiency (PCE) based on a newly designed semiconducting selenophene-thienopyrrolodione (TPD) copolymer blended with [6,6]-phenyl C_{71} butyric acid methyl-ester. The solar cells are fabricated using simple solution processing (implying low-cost fabrication). The relatively deep highest occupied molecular orbital (HOMO) level leads to a correspondingly high open-circuit voltage of 0.88 V. The PCE approaches 5.8% when Clevious P VP AI4083 is used as the hole-transport interlayer, with an optimized active layer thickness of approximately 95 nm, and a donor-acceptor blend ratio of 1:1. A fill factor (FF) of 0.62 is achieved. The use of additives does not seem to be beneficial in this blended system, due to the achievement of proper phase separation in the as-cast films. Also, the BHJ devices with a 3% ratio of a 1-chloronaphthalene (CN) additive exhibit much more severe oxidative degradation from the decreased FF with a high series resistance than BHJ devices without additive. The selenophene-TPD based BHJ solar cell is a promising candidate for high-performance single cells with a low-cost additive-free fabrication and a long-term stable operation.

1. Introduction

Bulk-heterojunction (BHJ) solar cells with the blending of donor-acceptor polymers based on solution-processible fabrication have been broadly researched because of promising advantages such as light weight, cost-effective manufacturing, and the possibility of flexible large-area devices for future industrial applications.[1–10] There have been significant improvements in power conversion efficiency (PCE) in BHJ solar cells over recent years.[11–18]

The thieno[3,4-c]pyrrole-4,6-dione (TPD)-based copolymer is considered as a promising electron-donating unit because of the relatively high open-circuit voltage (V_{oc}) from the deep highest occupied molecular orbital (HOMO) level.[19] Recently, Wei's group reported BHJ solar cells with a high PCE using a copolymer of bi(dodecyl)thiophene as an electron donor and 2-ethylhexyl-substituted TPD as an electron-withdrawing group (PBTTPD) with [6,6]-phenyl C_{71}-butyric acid methyl ester ($PC_{71}BM$). The optimum performance required the use of a 1,6-diiodohexane (DIH) additive.[20] Other emerging candidate TPD copolymers are dithienosilole-TPD (PDTSTPD) and terthiophene-TPD (P(S)) (see the molecular structure in the Supporting Information, Figure S1). These copolymers when blended with a fullerene acceptor exhibited an improved PCE when 1,8-diiodo-octane (DIO) and 1-chloronaphthalene (CN) processing additives were added to the chlorobenzene (CB) solvent, respectively.[21,22] A recent paper reported efficient solar cells with polyselenopheno[3,4-b]selenophene and $PC_{71}BM$ that exhibited a PCE of 6.87% when 2% of the DIO additive was mixed with the CB host solvent. However, this material has a relatively complicated synthesis and a long time preparation time for the monomers.[23] Moreover, without processing additives, the previous materials exhibited a significant drop of device performance due to a non-optimized photocurrent density (J_{sc}) and fill factor (FF).

The BHJ morphology is typically critically related to the various types and quantities of additive used and to the ratios between the polymer and the solvents. Using phase-contrast transmission electron microscopy (TEM), we have studied the BHJ nanomorphology through the addition of a CN additive with several vol% ratios.[22,24] The processing additive played an important role of reducing the aggregated regions and removing the grain boundaries in BHJ films. Moreover, BHJ cells processed with the CN additive and combined with a TiO_x interlayer demonstrated a higher fill factor (FF).[22,25] However, BHJ solar cells based on TPD copolymers such as PDTSTPD, PBTTPD, and P(S) still exhibited a relatively low PCE and J_{sc} without processing with an optimum amount of additive.

Here, for the first time, we have synthesized a selenophene-TPD copolymer (designated as P(Se)). P(Se) was polymerized using a green and relatively low-cost polymerization method (the so-called direct heteroarylation polymerization) with a relatively deep HOMO level of –5.49 eV. An enhanced PCE was achieved from this newly designed P(Se) and $PC_{71}BM$ BHJ active layer with the potential advantage of additive-free simple processing conditions. With both an optimized hole-transport

Dr. D. H. Wang, Prof. A. J. Heeger
Center for Polymers and Organic Solids
University of California at Santa Barbara
Santa Barbara, California 93106-5090, USA
E-mail: ajhe@physics.ucsb.edu
Dr. A. Pron, Prof. M. Leclerc
Department of Chemistry Université Laval
Quebec City, QC, G1V 0A6, Canada

DOI: 10.1002/adfm.201202541

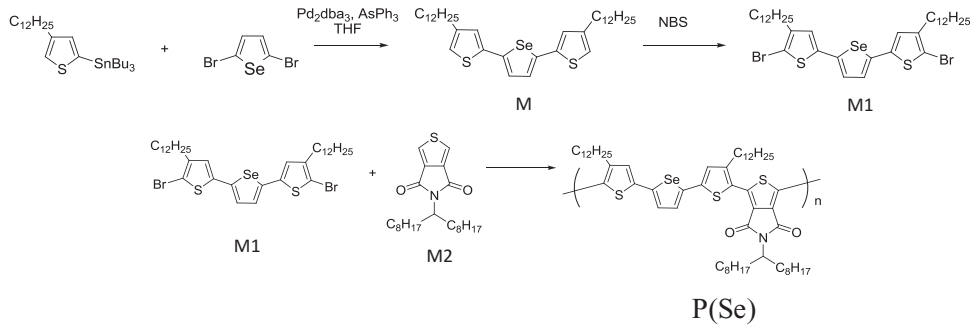

Figure 1. Synthesis steps and molecular structure of P(Se) from the monomers of M, M1, and M2 using a direct heteroarylation polymerization.

interlayer (HTL) and a BHJ active-layer thickness, the device exhibited an improved J_{sc} with a relatively high FF of 0.62, due to the well-defined nanomorphology and improved shunt resistance (R_{sh}). The use of the CN additive (3%) does not improve the performance; the CN additive induces a much higher efficiency decay in the P(Se):$PC_{71}BM$ BHJ devices (25% and 31% reduction), than observed in the additive-free BHJ devices (13% and 15% reduction) after 30 days in nitrogen (N_2) and in air, respectively.

2. Results and Discussion

2.1. Synthesis and Properties of the Newly Designed Selenophene-Thienopyrrolodione Copolymer

As shown in **Figure 1**, the TPD group is composed of bulky and alkyl branched side chains for inducing good solubility. We used a direct heteroarylation[26] procedure to synthesize the conjugated P(Se) which features selenophene as the electron-donating group and and TPD as the electron-accepting group. Monomers of 2,5-bis(4-dodecylthien-2-yl)selenophene (M), 2,5-bis(4-dodecyl-5-bromo-thien-2-yl)selenophene (M1), and 5-(9-heptadecanyl)-4H-thieno[3,4-c]pyrrole-4,6(5H)-dione (M2) were sequentially prepared using conventional organic solvents and room-temperature conditions.

To synthesize P(Se), M1 (103.4 mg, 0.13 mmol), M2 (51.28 mg, 0.13 mmol), *trans*-di(μ-acetato)bis[*o*-(di-*o*-tolyl-phosphino)benzyl]dipalladium(II) (2.7 mg, 4% mol), tris(*o*-methoxyphenyl)phosphine (4 mg, 8% mol), Cs_2CO_3 (160 mg, 0.35 mmol) and pivalic acid (7 mg, 0.04 mmol) were added to a Biotage microwave vial (2–5 mL) with a magnetic stirring bar. The vial was sealed with a cap and then purged with N_2 to remove the oxygen. 0.65 mL of tetrahydrofuran (THF) was added and the reaction was heated in an oil bath at 120 °C (reaction under pressure) for 22 h. After cooling to room temperature, the reaction mixture was poured in 250 mL of cold methanol. The precipitate was filtered. Soxhlet extractions with acetone followed by hexanes removed the catalytic residues and low-molecular-weight materials. The polymers were then extracted with chloroform. The solvent was reduced to about 7 mL and the mixture was poured into cold methanol. The selenophene-based TPD copolymer was achieved in a 94% yield as a soluble fraction in $CHCl_3$. Then, the high-molecular-weight copolymer was successfully prepared (M_n = 36 kDa, M_w = 71 kDa, PDI = 1.97). Details of the synthetic route are described in the Experimental Section and the molecular structures of M, M1, M2, and P(Se) are shown Figure 1.

In this study, a BHJ active layer was spin-cast between poly(3,4-ethylenedioxylenethiophene):poly(stylenesulfonate) (PEDOT:PSS) as a hole-transport interlayer (HTL) and an Al cathode, as shown in the device scheme of **Figure 2**a. As shown in the UV–vis spectra in Figure 2b, P(Se) shows a red-shift relative to P(S) during film solidification, whereas, in solution, the wavelengths for the maximum absorption were almost identical. Thus, an improved light harvesting of the solar spectrum by the BHJ films of P(Se) is expected because of absorption over a wider spectral range (see Figure 2b), and the film color is close to purple. Figure 2c shows the HOMO (–5.49 eV) and lowest unoccupied molecular orbital (LUMO) (–3.82 eV) energy levels of P(Se) as obtained by cyclic voltammetry (CV) (the CV data are shown in the Supporting Information, Figure S2). Furthermore, P(Se):$PC_{71}BM$ exhibits relatively high charge-carrier hole mobility of 0.017 $cm^2 V^{-1} s^{-1}$ as obtained from measurements of field-effect transistors (FETs); the data are shown in the Supporting Information, Figure S3.

Ultraviolet photoelectron spectroscopy (UPS) was used to characterize the P(Se):$PC_{71}BM$ BHJ film and to confirm the energy levels of the blended film. **Figure 3**a shows the UPS results for P(Se):$PC_{71}BM$ BHJ on top of an inidum tin oxide (ITO) substrate. Analysis of the secondary electron cut-off region in Figure 3a,b (14–19 eV) makes it possible to extract the shift in the vacuum energy level (E_{vac}); the E_{vac} shift is a measure for the magnitude of the interfacial dipole (Δ).[27–31] The deposition of a blend BHJ layer leads to a shift toward higher binding energies. The blend HOMO energy levels (E_{HOMO}) were determined using the low-binding-energy region (0–3 eV). The hole-injection barrier (Φ_h) is the energy difference between the E_{HOMO} and zero binding energy; from Figure 3b, Φ_h = 0.69 eV for P(Se):$PC_{71}BM$. Thus, the introduction of the $PC_{71}BM$ acceptor changes the E_{HOMO} of P(Se):$PC_{71}BM$ BHJ film to –5.07 eV; then, the separated hole charge carriers can transfer from the HOMO energy of the BHJ to the ITO anode (–4.7 eV), as shown in Figure 3b.

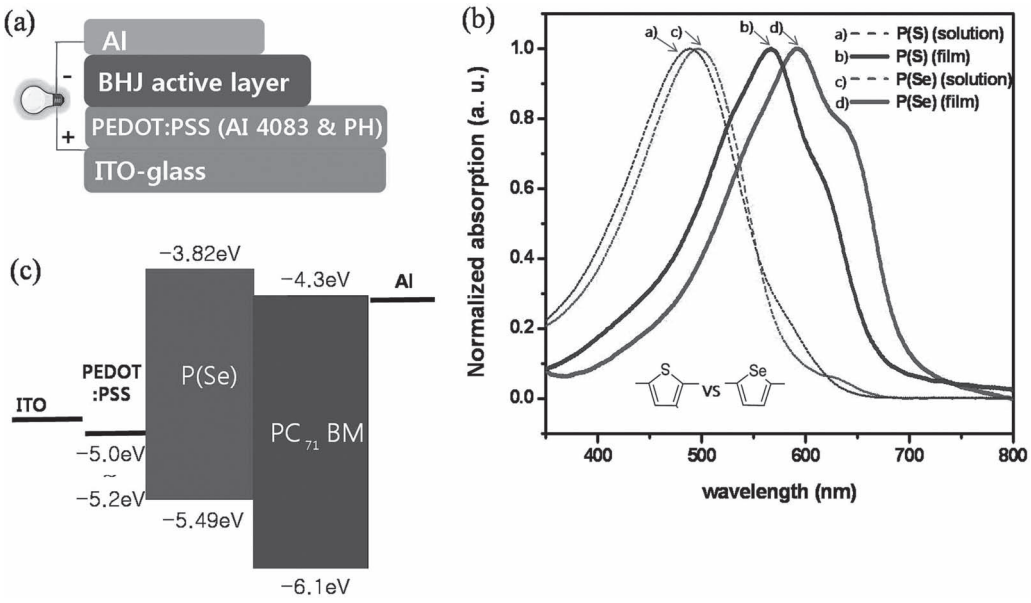

Figure 2. a) Schematic of P(Se):$PC_{71}BM$ BHJ polymer solar cells with different hole-transport interlayers of PEDOT:PSS (Clevious P VP AI4083 and Clevious PH). b) Normalized UV–vis absorption spectra of P(Se) and P(S). c) Energy-level diagram of P(Se) and $PC_{71}BM$.

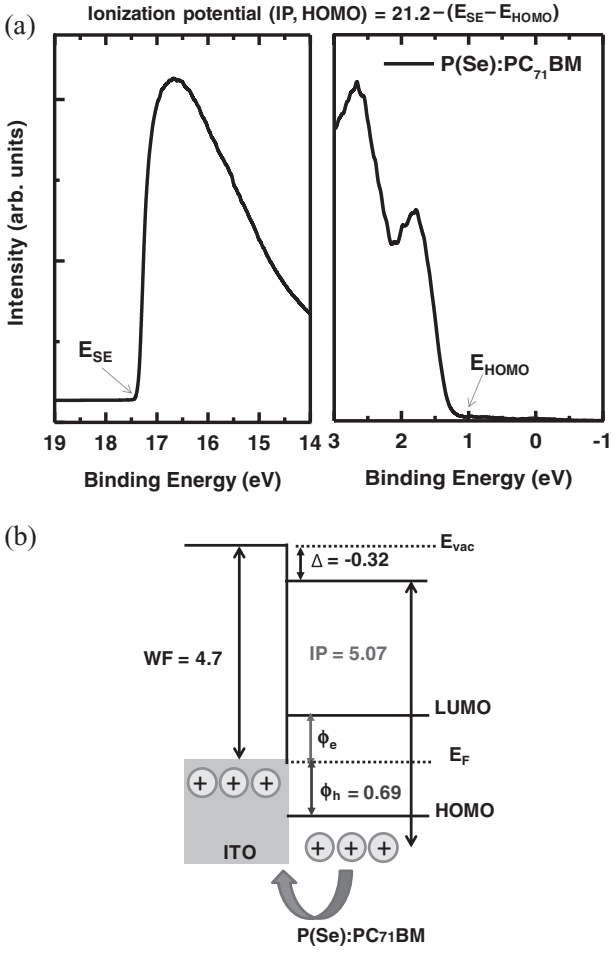

Figure 3. a) UPS spectra and b) energy diagrams of P(Se):$PC_{71}BM$ BHJ (E_{vac}: vacuum level, E_F: Fermi level, Δ: interfacial dipole, Φ_h: hole-injection barrier).

2.2. Optimization of Device Performances and Stability Comparison Between BHJ Solar Cells With and Without Additive

In order to optimize the P(Se):$PC_{71}BM$ BHJ solar cells, different HTLs of PEDOT:PSS were used between the ITO and the BHJ active layer. **Figure 4**a,b show the current-density–voltage (J–V) curves of the ratio-controlled P(Se) and $PC_{71}BM$ BHJ solar cells with different commercial brands of PEDOT:PSS – Clevious P VP AI4083, and Clevious PH, respectively. All of the devices were dissolved in 1,2-dichlorobenzene (DCB) solvents and were without any additives, to confirm the characteristics of the newly designed selenophene-based TPD copolymer. Figure 4c shows the incident photocurrent conversion efficiency (IPCE) corresponding to the data in Figure 4a. The performance of the P(Se):$PC_{71}BM$ BHJ solar cells is directly related to the HTL because of the simplicity of the cell architecture (only the PEDOT interlayer is used in this fabrication). For this reason, the quality of the HTL affects the optimized PCE efficiency parameters, and the BHJ nanomorphology.

The BHJ solar cells with Clevious P VP AI4083 (≈–5.2 eV to –5.0 eV) show a more-stable open-circuit voltage (V_{oc}), photocurrent density (J_{sc}), and FF values than the devices with Clevious PH (≈–4.8 eV to –5.0 eV). Because of the slightly deeper work function (WF) of Clevious P VP AI4083, it is well matched with the HOMO level of P(Se), which results in an efficient transport of separated hole charge carriers to the ITO electrode.[32,33] The well-defined BHJ nanomorphology is shown in the atomic force microscopy (AFM) images presented in **Figure 5**. The cells fabricated with Clevious P VP AI4083 show smooth surfaces with a root mean square (rms) roughness of 2.1 nm. The cells fabricated with Clevious PH, however, show smooth surfaces with an rms roughness of

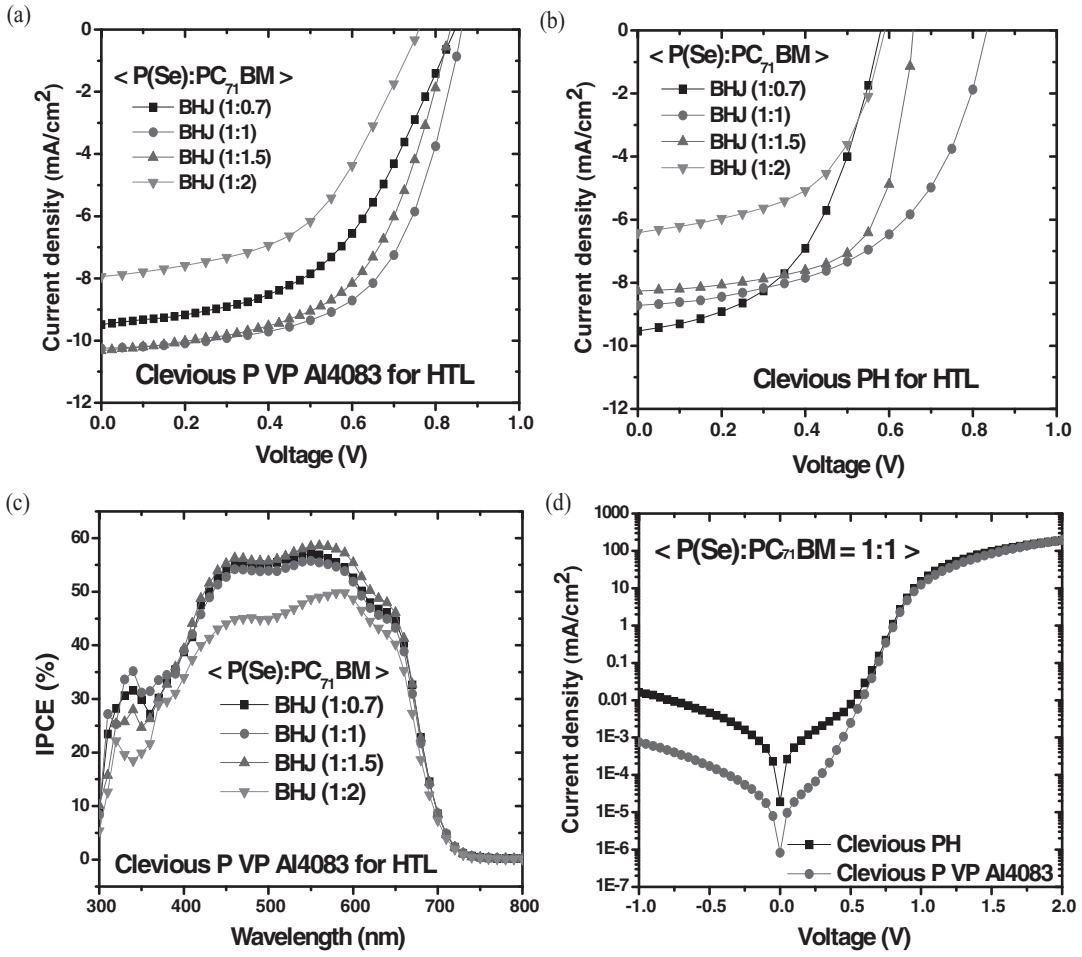

Figure 4. *J–V* curves of P(Se):PC_{71}BM BHJ solar cells based on different HTLs: a) Clevious P VP AI4083 and b) Clevious PH, with various donor and acceptor ratios. c) IPCE spectra of the devices with Clevious P VP AI4083. d) *J–V* curves of the devices at max. PCE for a 1:1 blend ratio with Clevious PH and P VP AI4083 in the dark.

3.0 nm. Moreover, as shown in the *J–V* curves (obtained in the dark) in Figure 4d, the 1:1 blend ratio of P(Se):PC_{71}BM BHJ with Clevious P VP AI4083 exhibits a higher shunt resistance (R_{sh}) and a reduced series resistance (R_s), compared with the Clevious PH. Thus, as shown in **Table 1**, an enhanced PCE of 5.30% (V_{oc} = 0.86 V, J_{sc} = 10.24 mA cm^{-2}, FF = 0.60) was achieved using Clevious P VP AI4083 compared with that obtained using Clevious PH: PCE = 3.88% (V_{oc} = 0.83 V, J_{sc} = 8.72 mA cm^{-2}, FF = 0.53).

Figure 6a shows the PCE thickness dependence of the BHJ active layer. To optimize the PCE of P(Se):PC_{71}BM BHJ solar cells, the thicknesses were changed from 75 nm, to 95 nm, 130 nm, and 200 nm depending on different spin-coating conditions. The BHJ cell with the 95 nm thickness (1500 rpm for 40 s) exhibits an optimized PCE of 5.80% (V_{oc} = 0.88 V, J_{sc} = 10.74 mA cm^{-2}, and FF = 0.62). The corresponding IPCE data are shown in the inset to Figure 6a. At a thickness of 200 nm, the PCE decreased to 4.09% (V_{oc} = 0.84 V, J_{sc} = 9.79 mA cm^{-2}, and FF = 0.50). The P(Se):PC_{71}BM BHJ solar cells have the tendency of having a reduced V_{oc}, J_{sc} and FF when the active-layer thickness is larger than 130 nm, as shown in Figure 6b–d and **Table 2**.

Although it is known from previous research that processing additives lead to a well-defined BHJ nanomorphology due to the reduction of the aggregations and the removal of the grain boundaries, interestingly the additive (CN) does not improve the performance in the P(Se):PC_{71}BM BHJ cells. When the processing additives are added in well-blended systems such as P(Se):PC_{71}BM, the BHJ may develop a non-optimized phase separation (perhaps as a result of excessive intermixing between the P(Se) and PC_{71}BM). The reduced performance of the P(Se):PC_{71}BM BHJ cells fabricated with CN (3%) is evident in the data of **Figure 7** and **Table 3**. The PCE drop is caused by the decreased FF from 0.62 to 0.43 when the 3% CN additive is blended with the BHJ active solutions.

Finally, we carried out stability tests of the P(Se):PC_{71}BM BHJ solar cells by normalized PCE and IPCE measurements, as shown in **Figures 8**a,b. The data were obtained from cells fabricated with an HTL of Clevious P VP AI4083 both with and without 3% CN additives as a function of time (day) in

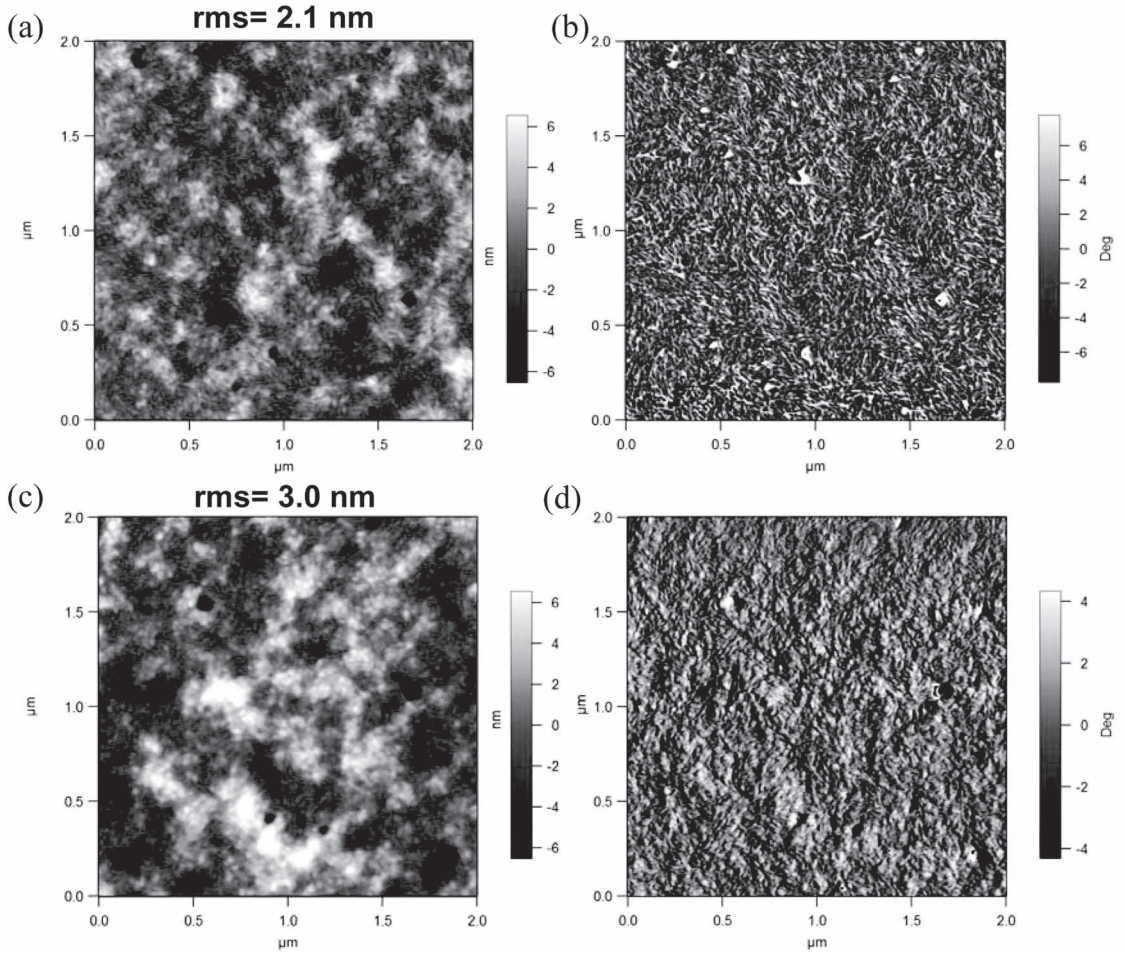

Figure 5. AFM images of: a,b) P(Se):$PC_{71}BM$ with Clevious P VP AI4083, and c,d) P(Se):$PC_{71}BM$ with Clevious PH without additive in BHJ films. (a) and (c) are height images; (b) and (d) are phase images (scan size: 2 µm × 2 µm).

N_2 and in air, respectively. After 30 days, the BHJ solar cells without additive (relatively smooth surface, rms roughness of 2.9 nm) showed efficiency decays of only 13% and 15% in N_2 and air, respectively. For the BHJ fabricated with 3% CN additives (rms roughness of 4.4 nm), 25% and 31% efficiency decays in the reduced IPCE data showed in N_2 and in air, respectively, from Figure 8a and the AFM images in the Supporting Information, Figure S4. The increased rms values of the BHJ with 3% CN additives arise from unwanted morphological changes due to the severe non-optimized phase separation that occurs as a function of storage time. In particular, the reduced FF is a critical factor in the significant PCE drop and efficiency decay after 30 days in air.[34,35] The BHJs fabricated with 3% CN additives exhibit a much larger decrease in PCE and FF from 3.06% to 2.12% and from 0.51 to 0.39, respectively, than BHJ solar cells without additive, from 5.36% to 4.56% and from 0.63 to 0.57, respectively, as shown in **Table 4**. The sharply reduced FF value of the BHJ devices with CN additive (3%) can be explained by severe oxidative degradation of the BHJ films, which exhibit a higher series resistance value of 17.4 Ω cm^2 than BHJ solar cells without additive of 4.15 Ω cm^2 after 30 days in air, from *J–V* curves in the dark, as shown in the Supporting Information, Figure S5. Thus, the additive-free nonpackaged P(Se):$PC_{71}BM$ BHJ solar cells exhibit a relatively long-term stable operation (in N_2 and in air) over 30 days without any passivation and electron-transport interlayer between the BHJ active layer and the cathode.

Table 1. Device processing conditions and efficiency parameters of P(Se):$PC_{71}BM$ BHJ solar cells with various donor and acceptor blend ratios (1:0.7, 1:1, 1:1.5, and 1:2).

Conditions of processing	P(Se):$PC_{71}BM$	V_{oc} [V]	J_{sc} [mA cm^{-2}]	FF	PCE [%]
PEDOT:PSS-Clevious P VP AI4083	1:0.7	0.85	9.49	0.50	4.02
Solvent: DCB	1:1	0.86	10.24	0.60	5.30
Additive: None; BHJ thickness = 130 nm	1:1.5	0.84	10.32	0.57	4.90
Cell Area = 11.76 mm^2	1:2	0.76	7.94	0.51	3.08

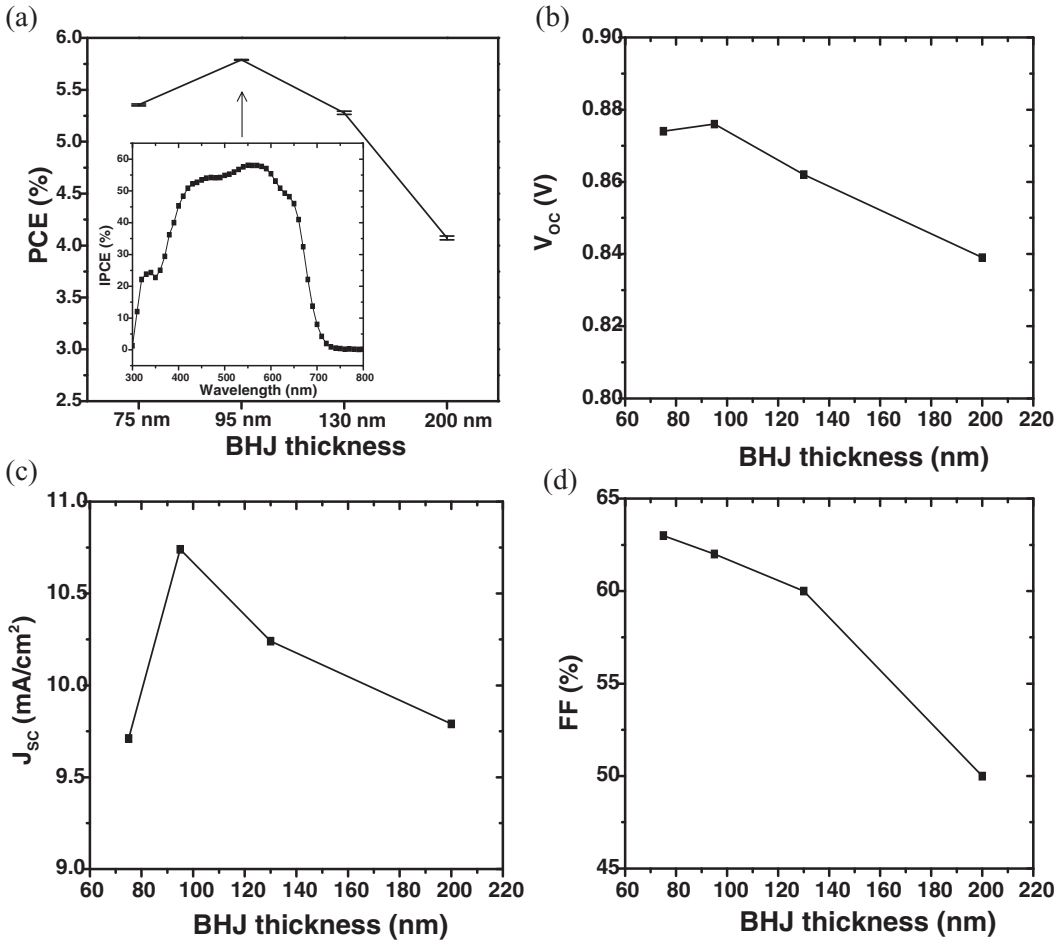

Figure 6. a) PCE as a function of the thickness of the BHJ active layer (the inset Figure shows the IPCE of the optimized BHJ thickness of 95 nm). b) V_{oc}, c) J_{sc}, and d) FF of the P(Se):$PC_{71}BM$ BHJ solar cells depending on the various active-layer thicknesses.

3. Conclusions

In summary, we fabricated additive-free BHJ solar cells using a newly designed semiconducting selenophene-based thieno[3,4-c]pyrrole-4,6-dione (TPD) alternating copolymer with a relatively deep HOMO level and an induced improved solubility by using direct heteroarylation reactions. Furthermore, the P(Se):$PC_{71}BM$ BHJ solar cells exhibit FF = 0.62, using Clevious P VP AI4083 with an optimized active-layer thickness (95 nm) and a donor-acceptor blend ratio of 1:1. Because of the original

Table 2. Device efficiency parameters and average efficiency of the P(Se):$PC_{71}BM$ BHJ solar cells, which depend on the active layer thicknesses, at a blend ratio of 1:1.

P(Se):$PC_{71}BM$ BHJ thickness [nm]	V_{oc} [V]	J_{sc} [mA cm^{-2}]	FF	PCE [%]	Average PCE [%]
75	0.87	9.71	0.63	5.36	5.35
95	0.88	10.74	0.62	5.80	5.79
130	0.86	10.24	0.60	5.30	5.28
200	0.84	9.79	0.50	4.09	4.07

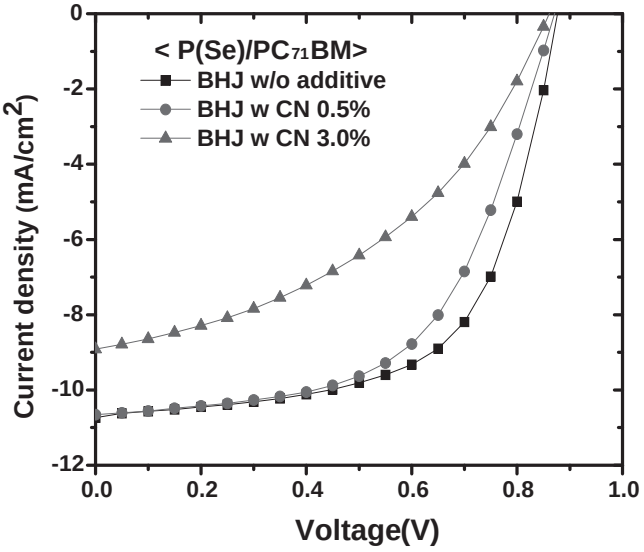

Figure 7. *J–V* curves of P(Se):$PC_{71}BM$ BHJ solar cells without an additive, and with the CN additive (0.5% and 3%) in DCB.

Table 3. Device processing conditions and efficiency parameters of a 1:1 blend ratio of the P(Se):$PC_{71}BM$ BHJ solar cells with and without a CN additive (0.5% and 3.0%) in DCB.

Conditions of processing	Additive	V_{oc} [V]	J_{sc} [mA cm^{-2}]	FF	PCE [%]
PEDOT:PSS-Clevious P VP AI4083	None	0.88	10.74	0.62	5.80
Solvent: DCB; P(Se):$PC_{71}BM$ = 1:1	CN 0.5%	0.87	10.66	0.57	5.27
Cell Area = 11.76 mm^2	CN 3.0%	0.86	8.91	0.43	3.27

Table 4. Device efficiency parameters, and efficiency-decay ratio (%) of the 1:1 blend ratio of P(Se):$PC_{71}BM$ BHJ solar cells with and without the CN (3%) additive as a function of storage time (as-cast and after 30 days) in N_2 and in air, respectively.

Additive	Conditions		V_{oc} [V]	J_{sc} [mA cm^{-2}]	FF	PCE [%]	Efficiency decay [%]
None	In N_2	As-cast	0.88	10.74	0.62	5.80	
		After 30 days	0.85	10.65	0.55	5.03	13
	In air	As-cast	0.87	9.71	0.63	5.36	
		After 30 days	0.86	9.29	0.57	4.56	15
CN (3%)	In N_2	As-cast	0.86	8.91	0.43	3.27	
		After 30 days	0.86	7.74	0.37	2.44	25
	In air	As-cast	0.72	8.40	0.51	3.06	
		After 30 days	0.63	8.57	0.39	2.12	31

good intermixing and proper phase separation between the P(Se) and the $PC_{71}BM$, the additive (CN) effects are negligible in this blended system. The BHJ solar cells fabricated with 3% CN additives exhibit much more severe oxidative degradation after 30 days than BHJ solar cells without additive, due to reduced FF with higher series resistance. Even though without any passivation or electron-transport interlayer, the nonpackaged BHJ solar cells exhibit a relatively long-term stability: over a period of 30 days, the losses in efficiency were only 13% and 15% when the cells were stored in nitrogen (N_2) and in air, respectively. The selenophene-TPD-based BHJ solar cell is an encouraging candidate for high-performance single cells that can be fabricated with low-cost and without the need for the use of processing additives.

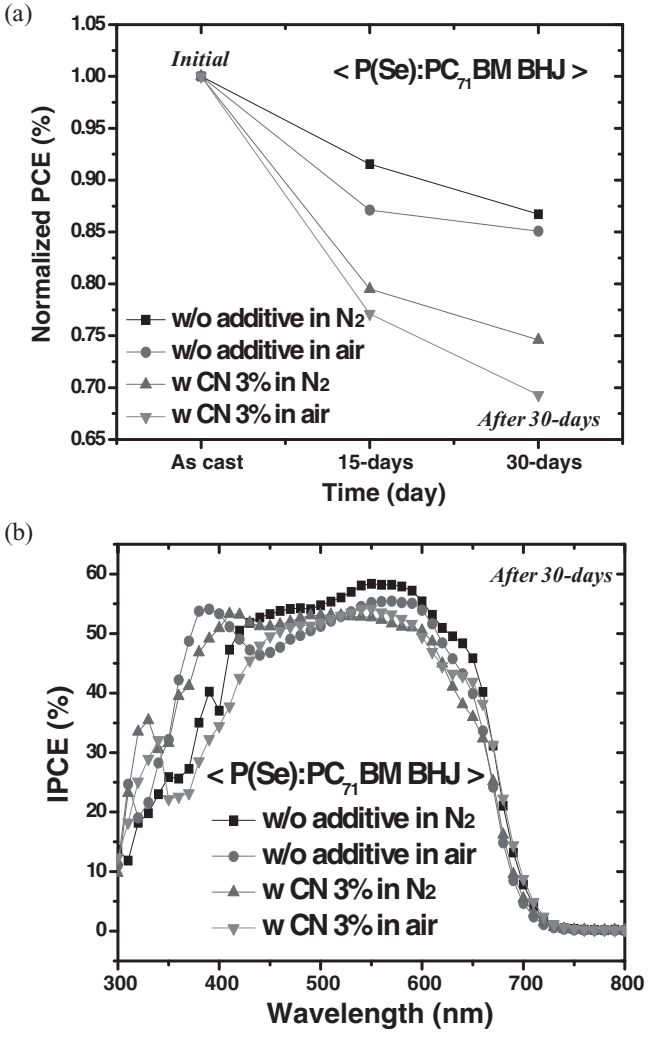

Figure 8. a) Normalized PCE from device-stability test as a function of time (day). b) IPCE after 30 days with and without CN (3%) additive (in days stored in N_2 and in air without packaging).

4. Experimental Section

Preparation of Monomers: We firstly synthesized the newly designed monomers and polymers by a selenophene substitution through direct heteroarylation polymerization reactions in a green and relatively low-cost method.[26]

2,5-Bis(4-dodecylthien-2-yl)selenophene (M): 2-(Tributylstannyl)-4-dodecylthiophene (2.81 g, 5.19 mmol) and 2,5-dibromoselenophene (0.60 g, 2.08 mmol) were dissolved in dry tetrahydrofuran (THF) (20 mL). The mixture was degassed. $Pd_2(dba)_3$ (0.060 g, 4% mol) and $AsPh_3$ (0.085 g, 16% mol) were added and the mixture was refluxed for 5 h. After cooling to room temperature, the solvent was evaporated and the crude compound was purified by column chromatography (silica gel) using hexanes as the eluent. The product was further purified by precipitation from cold acetone to achieve a pure sample of the title compound (0.42 g, 32% yield) as a light-yellow solid. ^{1}HNMR (400 MHz, $CDCl_3$, δ): 7.18 (s, 2H), 6.94 (s, 2H), 6.80 (s, 2H), 2.57 (t, 4H, J = 7.8Hz), 1.71–1.58 (m, 4H), 1.41–1.18 (m, 36H), 0.89 (t, 6H, J = 7.4Hz). ^{13}C NMR (100 MHz, $CDCl_3$, δ): 144.42, 141.39, 139.26, 126.21, 125.83, 119.49, 32.17, 30.74, 30.62, 29.97, 29.91, 29.84, 29.70, 29.61, 29.56, 22.94, 14.38 (some peaks overlap).

2,5-Bis(4-dodecyl-5-bromo-thien-2-yl)selenophene (M1): 2,5-bis(4-dodecylthien-2-yl)selenophene (0.095 g, 0.15 mmol) was dissolved in 6 mL of a chloroform/acetic acid mixture (2:1) and cooled at 0 °C. *N*-Bromosuccinimide (NBS) (0.054 g, 0.302 mmol) was added in one portion and reaction mixture was stirred in the dark for 1 h at 0 °C. The reaction was quenched by adding water. The organic phase was separated and washed with saturated solution of NaOH, dried over $MgSO_4$, and evaporated. The pure product was obtained as a yellow solid (0.104 g, 88%). ^{1}HNMR (400 MHz, $CDCl_3$, δ): 7.10 (s, 2H), 6.78 (s, 2H), 2.52 (t, 4H, J = 7.7 Hz), 1.63–1.54 (m, 4H), 1.35–1.20 (m, 36H), 0.89 (t, 6H, J = 7.4 Hz). ^{13}C NMR (100 MHz, $CDCl_3$, δ): 143.33, 140.72, 138.78, 126.50, 125.33, 108.45, 32.18, 29.93, 29.90, 29.89, 29.81, 29.65, 29.61, 29.46, 22.95, 14.38 (some peaks overlap).

5-(9-Heptadecanyl)-4H-thieno[3,4-c]pyrrole-4,6(5H)-dione (M2): M2 was prepared according to the reported procedures described by Jo et al.[22]

Fabrication of BHJ Solar Cells: The ITO-glass substrate was prepared by a cleaning process using detergent, acetone, and isopropyl alcohol. Then, the ITO was treated by UV-ozone (20 min) to re-form the surface, and then different commercial hole-transporting layers of PEDOT:PSS of Clevious PH and Clevious P VP AI 4083 were spin-coated on top of the ITO with a thickness of ≈35 nm. The ITO with the PEDOT:PSS was dried at 140 °C for 10 min, and then directly transferred to a glovebox to spin-cast the BHJ solution. Solutions with a total BHJ blend ratio of 30 mg ml^{-1} were prepared by dissolving the P(Se) and $PC_{71}BM$ in DCB depending on donor and acceptor ratios of 1:0.7, 1:1, 1:1.5, and 1:2 without any additives. The solution was stirred at 250 rpm and 60 °C on a hotplate. To get the optimized efficiency and processing conditions, solar cells were fabricated with several active-layer thicknesses from 75 nm to 200 nm. The BHJ layer was dried at 80 °C for 10 min to evaporate any residual solvents. Finally, an Al cathode (≈100 nm thickness) was thermally deposited under a vacuum pressure of 3×10^{-6} Torr.

Measurement and Characterization of BHJ Solar Cells: The encapsulation of the BHJ solar cells was performed using UV-curable epoxy and a cover-glass in a N_2 glovebox. Then, the *J–V* curves were measured using a Keithley 236 source measure unit, during which the solar cells were exposed to an intensity of 100 mW cm^{-2} after calibration of the light source with an AM 1.5 Global. An aperture of 11.76 mm^2 was used on top of the deposited Al cathode to determine the accurate cell area and to prevent an overestimation of the PCE. The BHJ surface morphology and roughness were observed by AFM (Veeco, USA; D3100). The IPCEs were measured using a quantum-efficiency (QE) measurement system (PV measurements, Inc.) to match and confirm the *J–V* characteristics after the calibration of the monochromatic power density. Bottom-contact organic FETs were fabricated on doped n-type silicon wafers with a SiO_2 dielectric layer. The Au source and drain electrodes were evaporated through an e-beam process with a channel length (*L*) of 20 μm and width (*W*) of 1000 μm in a clean room. The P(Se):$PC_{71}BM$ was dissolved in DCB (30 mg ml^{-1}) and was spin-coated on top of the substrate as shown in the inset to Figure S3 in the Supporting Information. The films were dried at 80 °C for 10 min. The electric measurements were carried out using a Signatone probe station and a Keithley 4200 system within a N_2-atmosphere glovebox.

Supporting Information

Supporting Information is available from the Wiley Online Library or from the author.

Acknowledgements

The research at UCSB and Laval University was supported by the US Army General Technical Services (GTS/GTS-S-11-321). The authors also thank Dr. Mike Tseng, Jason Seifter, and Prof. J. H. Seo for their helpful assistance.

Received: September 5, 2012
Published online: October 16, 2012

[1] N. S. Sariciftci, L. Smilowitz, A. J. Heeger, F. Wudl, *Science* **1992**, *258*, 1474–1476.
[2] G. Yu, J. Ga, J. C. Hummelen, F. Wudl, A. J. Heeger, *Science* **1995**, *270*, 1789–1791.
[3] A. J. Heeger, *Angew. Chem. Int. Ed.* **2001**, *40*, 2591–2611.
[4] C. J. Brabec, N. S. Sariciftci, J. C. Hummelen, *Adv. Funct. Mater.* **2001**, *11*, 15–26.
[5] S. H. Park, A. Roy, S. Beaupré, S. Cho, N. Coates, J. S. Moon, D. Moses, M. Leclerc, K. Lee, A. J. Heeger, *Nat. Photonics* **2009**, *3*, 297–303.
[6] Y. Liang, Z. Xu, J. Xia, S.-T. Tsai, Y. Wu, G. Li, C. Ray, L. Yu, *Adv. Mater.* **2010**, *22*, E135–E138.
[7] Z. Yin, S. Sun, T. Salim, S. Wu, X. Huang, Q. He, Y. M. Lam, H. Zhang, *ACS Nano* **2010**, *4*, 5263–5268.
[8] S. R. Cowan, N. Banerji, W. L. Leong, Alan J. Heeger, *Adv. Funct. Mater.* **2012**, *22*, 1116–1128.
[9] X. Li, W. C. H. Choy, L. Huo, F. Xie, W. E. I. Sha, B. Ding, X. Guo, Y. Li, J. Hou, J. You, Y. Yang, *Adv. Mater.* **2012**, *24*, 3046–3052.
[10] S. Kouijzer, S. Esiner, C. H. Frijters, M. Turbiez, M. M. Wienk, R. A. J. Janssen, *Adv. Energy Mater.* **2012**, *2*, 945–949.
[11] L. Huo, S. Zhang, X. Guo, F. Xu, Y. Li, J. Hou, *Angew. Chem. Int. Ed.* **2011**, *50*, 9697–9702.
[12] D. H. Wang, D. Y. Kim, K. W. Choi, J. H. Seo, S. H. Im, J. H. Park, O. O. Park, A. J. Heeger, *Angew. Chem. Int. Ed.* **2011**, *50*, 5519–5523.
[13] J. Yang, J. You, C.-C. Chen, W.-C. Hsu, H.-R. Tan, X. W. Zhang, Z. Hong, Y. Yang, *ACS Nano* **2011**, *5*, 6210–6217.
[14] C. E. Small, S. Chen, J. Subbiah, C. M. Amb, S.-W. Tsang, T.-H. Lai, J. R. Reynolds, F. So, *Nat. Photonics* **2012**, *6*, 115–120.
[15] D. H. Wang, J. S. Moon, J. Seifter, J. Jo, J. H. Park, O. O. Park, A. J. Heeger, *Nano Lett.* **2011**, *11*, 3163–3168.
[16] V. S. Gevaerts, A. Furlan, M. M. Wienk, M. Turbiez, R. A. J. Janssen, *Adv. Mater.* **2012**, *24*, 2130–2134.
[17] L. Dou, J. You, J. Yang, C.-C. Chen, Y. He, S. Murase, T. Moriarty, K. Emery, G. Li, Y. Yang, *Nat. Photonics* **2012**, *6*, 180–185.
[18] D. H. Wang, J. Seifter, J. H. Park, D.-G. Choi, A. J. Heeger, *Adv. Energy Mater.* DOI: 10.1002/aenm.201200349.
[19] Y. Zou, A. Najari, P. Berrouard, S. Beaupré, B. R. Aïch, Y. Tao, M. Leclerc, *J. Am. Chem. Soc.* **2010**, *132*, 5330–5331.
[20] M.-S. Su, C.-Y. Kuo, M.-C. Yuan, U.-S. Jeng, C.-J. Su, K.-H. Wei, *Adv. Mater.* **2011**, *23*, 3315–3319.
[21] T.-Y. Chu, J. Lu, S. Beaupé, Y. Zhang, J.-R. Pouliot, S. Wakim, J. Zhou, M. Leclerc, Z. Li, J. Ding, Y. Tao, *J. Am. Chem. Soc.* **2011**, *133*, 4250–4253.
[22] J. Jo, A. Pron, P. Berrouard, W. L. Leong, J. D. Yuen, J. S. Moon, M. Leclerc, A. J. Heeger, *Adv. Energy Mater.* DOI: 10.1002/aenm.201200350.
[23] H. A. Saadeh, L. Lu, F. He, J. E. Bullock, W. Wang, B. Carsten, L. Yu, *ACS Macro Lett.* **2012**, *1*, 361–365.
[24] J. S. Moon, C. J. Takacs, S. Cho, R. C. Coffin, H. Kim, G. C. Bazan, A. J. Heeger, *Nano Lett.* **2010**, *10*, 4005–4008.
[25] S. Kwon, J. K. Park, G. Kim, J. Kong, G. C. Bazan, K. Lee, *Adv. Energy Mater.* DOI: 10.1002/aenm.201200311.
[26] P. Berrouard, A. Najari, A. Pron, D. Gendron, P.-O. Morin, J.-R. Pouliot, J. Veilleux, M. Leclerc, *Angew. Chem. Int. Ed.* **2012**, *51*, 2068–2071.
[27] S. Braun, W. R. Salaneck, M. Fahlman, *Adv. Mater.* **2009**, *21*, 1450–1472.
[28] I. G. Hill, D. Milliron, J. Schwartz, A. Kahn, *Appl. Surf. Sci.* **2000**, *166*, 354–362.
[29] J. H. Seo, R. Yang, J. Z. Brzezinski, B. Walker, G. C. Bazan, T.-Q. Nguyen, *Adv. Mater.* **2009**, *21*, 1006–1011.
[30] Y. Gao, *Acc. Chem. Res.* **1999**, *32*, 247–255.
[31] H. Ishii, K. Sugiyama, E. Ito, K. Seki, *Adv. Mater.* **1999**, *11*, 605–625.
[32] T.-W. Lee, O. Kwon, M.-G. Kim, S. H. Park, J. Chung, S. Y. Kim, Y. Chung, J.-Y. Park, E. Han, D. H. Huh, J.-J. Park, L. Pu, *Appl. Phys. Lett.* **2005**, *87*, 231106.
[33] The material information is available from the H. C. Starck and Heraeus websites, http://www.hcstarck.com/, and from http://clevios.com/en/home/clevios-homepage.aspx (accessed September 2012).
[34] D. H. Wang, J. K. Kim, J. H. Seo, O. O. Park, J. H. Park, *Sol. Energy Mater. Sol. Cells* **2012**, *101*, 249–255.
[35] D. H. Wang, J. K. Kim, O. O. Park, J. H. Park, *Energy Environ. Sci.* **2011**, *4*, 1434–1439.